


Article

Fabrication and Magneto-Optical Properties of Yb₂O₃ Based Ceramics

Dmitry A. Permin ^{1,2,*} , Anastasia V. Novikova ¹, Vitaly A. Koshkin ¹, Stanislav S. Balabanov ¹, Ilya L. Snetkov ^{2,3}, Oleg V. Palashov ^{2,3} and Ksenia E. Smetanina ²

¹ G.G. Devyatykh Institute of Chemistry of High-Purity Substances of the RAS, 603951 Nizhny Novgorod, Russia; novikova@ihps-nnov.ru (A.V.N.); dustchem@bk.ru (V.A.K.); balabanov@ihps-nnov.ru (S.S.B.)

² Research Institute for Physics and Technology, Lobachevsky State University of Nizhny Novgorod, 603950 Nizhny Novgorod, Russia; snetkov@appl.sci-nnov.ru (I.L.S.); palashov@appl.sci-nnov.ru (O.V.P.); smetanina@phys.unn.ru (K.E.S.)

³ Institute of Applied Physics of the Russian Academy of Sciences, 603950 Nizhny Novgorod, Russia

* Correspondence: permin@ihps-nnov.ru

Received: 16 October 2020; Accepted: 14 November 2020; Published: 16 November 2020



Abstract: Transparent ceramics based on ytterbium oxide have been successfully produced by vacuum sintering of self-propagating high-temperature synthesized powders with use of a La₂O₃ sintering aid. Phase composition and microstructure of the initial powders were studied by X-ray diffraction analysis and scanning electron microscopy. It was found that addition of 5 mol.% of La₂O₃ does not cause formation of secondary phases in the Yb₂O₃ powders. The 4% La:Yb₂O₃ ceramics showed the best in-line transmittance of 73% at a wavelength of 2 μm among the studied samples. Dependence of the Verdet constant on wavelength was investigated in the range of 0.4–2 μm. The most promising finding is use of the obtained material as Faraday isolators in the wavelength region of ~1.5 μm, where there are no absorption bands, and the Verdet constant is 8.6 rad/(T·m).

Keywords: Yb₂O₃; magneto-optical ceramics; SHS; vacuum sintering; Verdet constant

1. Introduction

The magnetic field causes a change in the dielectric tensor, which is responsible for the refractive index, absorption in the material, and various magneto-optical effects. One of these effects is the Faraday rotation of the polarization plane (circular birefringence). This effect is widely used for measuring the magnitude of the magnetic field, indirect determining the values of some parameters (for example, magneto-optical electric current sensors [1]), and various manipulations with the polarization of the transmitted radiation (Faraday devices, magneto-optical Q-switch modulators [2], choppers, polarization switches, deflectors [3], etc.).

Faraday isolators (FI) and rotators (FR) have found a wide application in laser physics. These devices are used to organize multi-pass amplifier schemes and schemes with a compensation for thermally induced birefringence of lasers active elements, for optical isolation of different parts of the laser scheme, and for ensuring propagation of laser radiation in a strictly specified direction.

Faraday isolator is an optical device, proposed in its traditional form by Lord Rayleigh. As shown in Figure 1, it represents a magneto-optical element (MOE) located between two polarizers (1,4) crossed relative to each other at the same angle and placed in an external magnetic field (3). MOE non-reciprocally rotates the polarization plane of the transmitted radiation by 45°. A half-wave plate (2) is often included in the FI scheme, which is tuned to rotate polarization in the direction opposite to the Faraday rotation at an angle of 45°, while the polarizers do not cross. This makes it possible to keep the direction of transmitted radiation polarization when the FI is introduced into it.

Due to the half-wave plate, in the absence of thermal effects polarization of radiation passing in the direction of the direct passage (from B to A) remains unchanged (for example, horizontal—parallel to the x -axis), and radiation passes through polarizer 4. On the backward passage (from A to B), polarization changes to vertical (parallel to the y -axis), and radiation is reflected by polarizer 1.

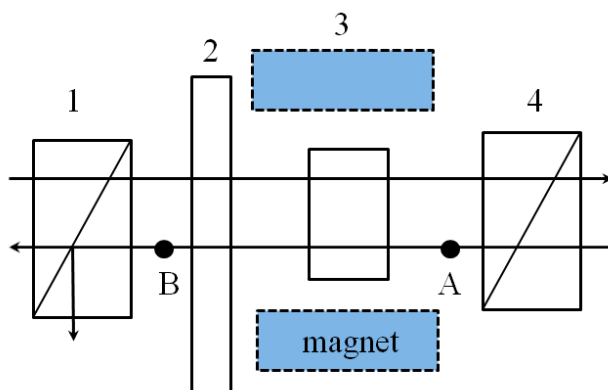


Figure 1. Conventional Faraday isolator circuit: 1,4—polarizers; 2— $\lambda/2$ plate; 3— 45° magneto-optical element (MOE).

A specific task is development of FI and FR for high average power lasers. Thermally induced effects arising from absorption in the magneto-optical element lead to inhomogeneous changes of transmitted radiation polarization. This worsens the main characteristics of Faraday devices—uniformity of polarization plane rotation (for FR) and isolation degree (for FI). Additionally, with increasing the power of transmitted radiation, the resulting thermal effects become stronger, worsening the performance of Faraday devices. At a certain power of laser radiation, the FI and FR no longer meet the requirements for isolation and uniformity of polarization rotation, and these devices need to be improved to advance into the high-power region. For this purpose, one could improve the magnetic system [4,5], use optical circuits with compensation for thermal effects [6–9], use optimal crystal orientations arising from dependence of thermal effects on the direction of crystallographic axes [10,11], and look for new magneto-optical materials.

The main efforts of researchers in the latter direction are aimed at developing new magneto-optical materials with better characteristics (high thermal conductivity and Verdet's constant, minimal absorption at operating wavelengths, etc.). Recently, ceramic technology for such material fabrication has been noted as one of the most promising developments, and on this basis a number of ceramics with unique characteristics have already been prepared [12–16]. Progress in development of large-size FIs, which are important for creation of high-power laser sources, can be related to use of rare-earth sesquioxides as a base material. Rare-earth oxides (REO) are very promising due to high concentrations of paramagnetic RE^{3+} ions in comparison with other materials. REO have a wide transparency range and excellent mechanical and thermal properties. It has recently been shown that Tb_2O_3 [17–19], Dy_2O_3 [20,21], and Ho_2O_3 [22–24] ceramics have a higher Verdet constant of 3.5, 2.2 and 1.3 times, respectively, in comparison with one of the widely used materials, a single crystal of terbium gallium garnet (TGG). Other studied ceramics based on rare-earth cubic oxides include Er_2O_3 [25], which has a low value of the Verdet constant and is of limited interest for magneto-optical applications, and diamagnetic RE^{3+} ion based ceramics (Y_2O_3 , Sc_2O_3 , Gd_2O_3 , and Lu_2O_3), which have even lower values. There are some data in literature on preparation of Yb_2O_3 in the form of single crystals and study of its optical properties [26]. Information on production of Yb_2O_3 optical ceramics in the available literature is limited to a single patent [27], and magneto-optical characteristics of ceramics based on ytterbium oxide have not been studied.

The aims of this work were to prepare transparent Yb_2O_3 ceramics by vacuum sintering of nanodispersed powders and to evaluate optical and magneto-optical characteristics, which are of decisive importance for their use in Faraday isolators and rotators.

2. Experimental

Powders of ytterbium oxide and mixed ytterbium-lanthanum oxides were obtained by self-propagating high-temperature synthesis (SHS), previously successfully used for preparation of other rare-earth nanopowders [28–33]. Ytterbium and lanthanum nitrates were used as an oxidant, and glycine was used as a reducing agent.

The starting materials were ytterbium oxide Yb_2O_3 (99.999% Yumeks, Russia), lanthanum oxide La_2O_3 (99.99% Polirit, Russia), nitric acid HNO_3 (99.9999%, Khimreaktiv, Russia), and glycine $\text{NH}_2\text{CH}_2\text{COOH}$ (99.9%, Khimreaktiv, Russia). Metal nitrates were obtained by dissolving ~10 g of starting metal oxides in a nitric acid under stirring and heating. The solution concentration was determined by weighting a dry residue after evaporation and calcination at a temperature of 1100 °C. Then the solutions were mixed according to the desired stoichiometry of the ytterbium-lanthanum oxides, and glycine was added in a molar ratio of 1:1 with respect to the metal nitrates. The resulting precursor solution was evaporated at a temperature of ~110 °C in a quartz flask, which was placed in a resistance furnace preheated to 300 °C. Heating of the precursor led to initiation of exothermic reactions and propagation of the SHS process over the entire volume of the charge. As a result, formation of highly dispersed white powders of ytterbium and ytterbium-lanthanum oxides occurred. The combustion process was accompanied by evolution of a large amount of gas-phase products. To ensure oxidation of organic by-products and desorption of water, the SHS-product was annealed at a temperature of 900 °C for 30 min. Powders of five compositions, Yb_2O_3 , 1% $\text{La}:\text{Yb}_2\text{O}_3$, 2% $\text{La}:\text{Yb}_2\text{O}_3$, 3% $\text{La}:\text{Yb}_2\text{O}_3$, 4% $\text{La}:\text{Yb}_2\text{O}_3$, and 5% $\text{La}:\text{Yb}_2\text{O}_3$, were prepared.

To obtain the ceramics, the powders were uniaxially pressed in \varnothing 15 mm disks under a pressure of 300 MPa. Sintering was carried out in a vacuum furnace at a temperature of 1750 °C for 3 h at a heating rate of 10 °C/min at a residual pressure of no more than 10^{-2} Pa. Then the ceramic samples were calcined in air at 900 °C for 2 h and mirror polished on both sides.

XRD patterns of the prepared powders were recorded with a Shimadzu XRD-7000 (Shimadzu, Japan) with a graphite monochromator (Cu ($K\alpha$ radiation $\lambda = 1.54178$ Å) in the 2θ range of 25–60° with a scanning step of 0.04°. Qualitative phase analysis was carried out using the “Diffrac.EVA” program. Presence of a particular phase in the samples was visually determined from the diffraction patterns obtained during the experiments using data from the PDF-2 powder diffraction bank. The average crystallite size of the powders was calculated from the peak broadening of the XRD pattern using Scherrer’s Equation (1):

$$d_{\text{XRD}} = 0.9 \lambda / B \cos \theta, \quad (1)$$

where B is the full width at half maximum (in 2θ), θ is the angle of the reflex maximum (in 2θ), and λ is the average wavelength (1.54 Å).

The powder morphology, ceramic microstructure, and average grain size were investigated using a JSM 6390 (JEOL, Japan) scanning electron microscope.

Density of the ceramic samples was calculated by hydrostatic weighing in water with an accuracy of 0.01 g/cm³.

Optical transmission spectra were recorded using a Shimadzu UV-3600 spectrophotometer in the ultraviolet, visible, and near infrared wavelength range (200–2000 nm) and a Fourier-transform infrared (FT-IR) spectrometer FSM 1201 (Infraspek, Russia) (1500–10,000 nm).

Dependence of the Verdet constant on a wavelength was measured by two approaches: using probe laser sources at wavelengths of 1064, 1310, 1550, and 1940 nm and using the polarization-stepping method in the range of 400–1100 nm [34]. The Verdet constant was measured at a temperature of 25 °C. Magneto-optical element was fixed in the center of a magnetic system, which was placed between two polarizers: calcite wedge and Glan prism. The magnetic field changed less than for 0.2% of the

value of 2.77 T over the length of the sample; thus, the magnetic field around the sample was uniform. Diode lasers at the wavelengths of 1310 and 1550 nm, and Nd:YAG (1064 nm) and Tm fiber (1940 nm) lasers were used as the probe laser sources. The Faraday rotation angle (θ) was determined by the angle of rotation of the Glan prism corresponding to the minimum signal on the camera in the absence and presence of a magnetic field.

Using the known values of the length of each studied sample L , the magnetic field B , and the Faraday rotation angle θ , the Verdet constant V was found at each probe wavelength. Avantes Avalight-hal-mini, generating in the 300–1400 nm wavelength range, was used as a broadband white light source of probe radiation for the polarization-stepping method. The Avantes AvaSpec Evo spectrometer was used as an analyzer of the transmitted radiation spectrum. The measurement range was determined by the white light source spectrum and the sensitivity of the scheme. The dependence of the Faraday rotation angle on wavelength was found by measuring the transmitted light spectrum intensity dependence on the Glan prism rotation in the presence and absence of a magnetic field.

3. Results and Discussion

Vacuum sintering of nanopowders with use of lanthanum oxide as a sintering aid is one of the most effective approaches in production of optical rare-earth oxides ceramics. For example, Y_2O_3 [28,29], Dy_2O_3 [20,21], Ho_2O_3 [23], Lu_2O_3 [30], and Er_2O_3 [25] ceramics were previously synthesized based on this approach. The action of lanthanum oxide in improvement of REO sinterability consists in increasing the number of point defects in the material, which accelerates mass transfer and causes rapid healing of pores. However, La_2O_3 has limited solubility in cubic REOs and tends to segregate along grain boundaries and form secondary phases. This leads to fluctuations in the refractive index in the sample volume and scattering of the transmitted radiation. Thus, it is important to select the concentration of lanthanum oxide in the material in order to prevent formation of secondary phases, but at the same time to provide sufficient improvement in sinterability to obtain pore-free material. In this regard, experiments on Yb_2O_3 sintering were carried out on a series of samples containing 0–5 mol.% La_2O_3 .

3.1. Properties of Yb_2O_3 Based Powders

Figure 2 shows SEM images of the glycine-nitrate-derived Yb_2O_3 and 5%La: Yb_2O_3 powders. The powders have a foamy structure with fine wall thicknesses and an effective agglomerates diameter of up to several microns. At that, lanthanum oxide addition does not noticeably affect the morphology of the resulting powders.

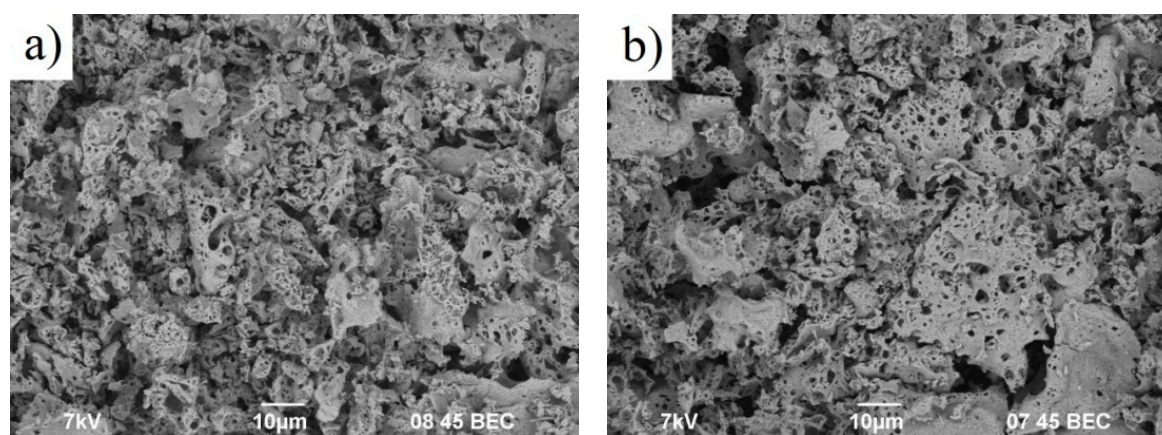
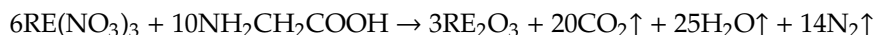


Figure 2. Micrographs of Yb_2O_3 (a) and 5%La: Yb_2O_3 (b) self-propagating high-temperature synthesis SHS powders.

The morphology of SHS powders is caused by the action of gaseous substances that disperse the batch and lead to production of crumbly white Yb_2O_3 . The corresponding equation of chemical reactions can be written as follows:



As revealed from XRD analysis (Figure 3a), the as-synthesized powders are a single-phase cubic Yb_2O_3 S.G.: $\text{Ia}\bar{3}$ (206) (PDF # 00-041-1106); impurities of other phases were not detected. The XRD crystallite size of the powders decreases with increasing the lanthanum oxide content. The concentration of La_2O_3 is close to the solubility limit in Yb_2O_3 , which probably explains why it interferes with powder crystallization. The lattice parameter linearly increases (Figure 3b) with the La_2O_3 concentration and corresponds to Vegard's law, but due to the high dispersity of the powders, errors in determining this value are significant. Therefore, it is difficult to affirm substitutional solid solutions of ytterbium and lanthanum oxide, which are formed in the powders. However, in Ho_2O_3 and Er_2O_3 powders, obtained under similar conditions, a significantly higher solubility of La_2O_3 was found in comparison with the literature data. This was explained by both the nanodispersed disordered structure of the powders and kinetic difficulties in formation of the second phase, since segregation of lanthanum ions does not have time to occur during the SHS process.

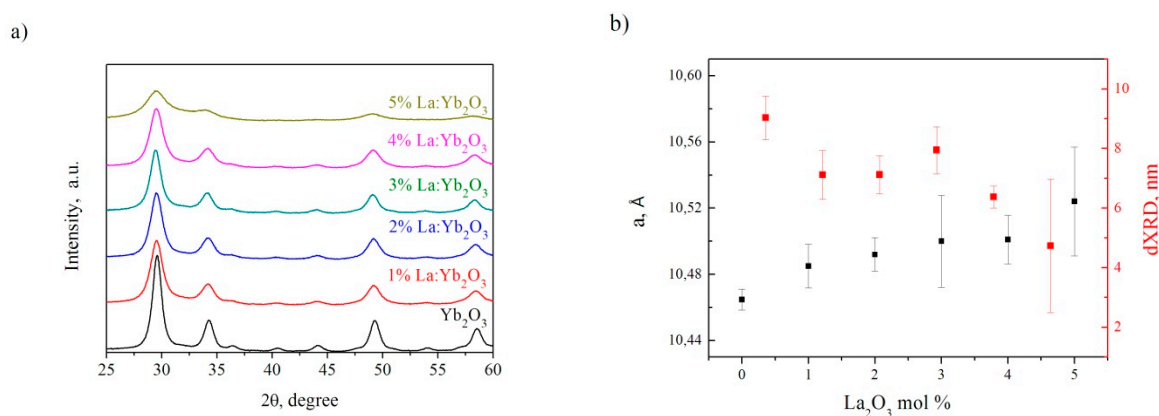


Figure 3. XRD patterns of Yb_2O_3 and 1–5% La_2O_3 : Yb_2O_3 powders (a) and dependence of a and d_{XRD} on the La_2O_3 content (b).

3.2. Sintering and Microstructure of $(\text{Yb}_x\text{La}_{1-x})_2\text{O}_3$ Ceramics

After vacuum sintering, partial reduction of Yb^{3+} ions occurred, which manifested in dark color. After oxidative annealing in air at 900 °C for 5 h, the samples became almost colorless.

Lanthanum oxide notably affects sintering of the ceramics, which is reflected in the ceramic microstructure. Figure 4 shows micrographs of the surface of the $(\text{Yb}_x\text{La}_{1-x})_2\text{O}_3$ ceramic samples. The Yb_2O_3 sample contains a number of pores at grain boundaries and at triple junctions. The density of individual Yb_2O_3 ceramics is about 97% of the theoretical value. A large number of pores is also observed in ceramics containing 1% of the La_2O_3 . With an increase in the lanthanum oxide content, a decrease in the porosity of the samples (2–3% La_2O_3) is observed. Samples with a sintering aid content of 4–5% are of almost the theoretical density; no pores could be seen on the ceramic surfaces. Lanthanum oxide does not cause significant grain growth in comparison with individual ytterbium oxide, as was in the case of sintering of lutetium-yttrium-lanthanum oxides solid solutions [30]. Mostly intragranular fracture was observed in ceramics regardless of lanthanum oxide content. This indicates the absence of displacement of any impurities from the grain volume, which weakens the grain boundaries. As seen on fractograms, segregations and other inhomogeneities, except for pores, are not found in ceramics.

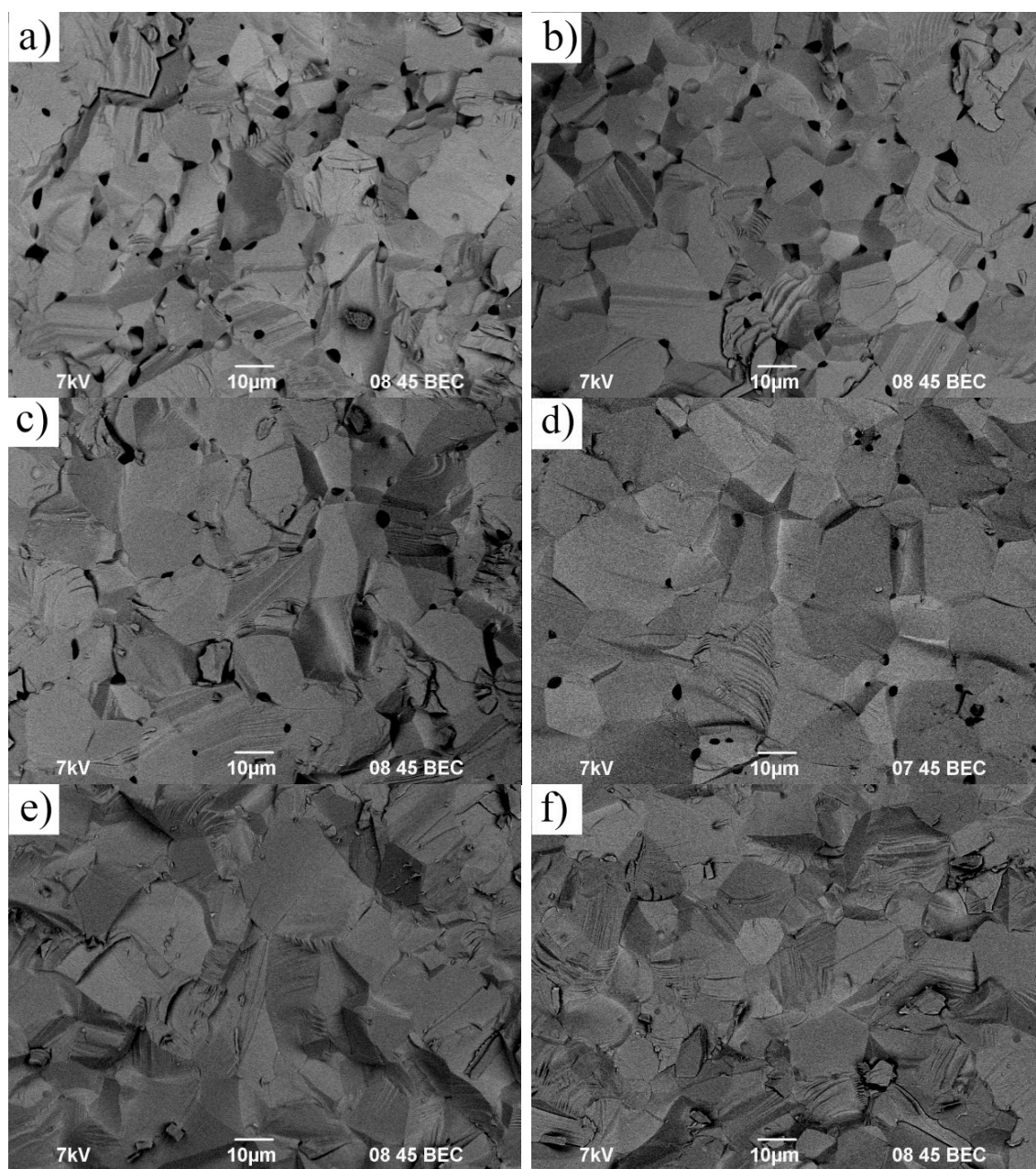


Figure 4. SEM images of Yb_2O_3 (a) and 1–5% $\text{La}:\text{Yb}_2\text{O}_3$ (b–f) ceramic sample fracture surfaces.

The appearance of the obtained ceramics based on Yb_2O_3 is shown in Figure 5. The 4% $\text{La}:\text{Yb}_2\text{O}_3$ ceramics show the highest level of transparency. When the sintering aid content is less than 4%, the light transmission of the ceramics is limited by scattering caused by the residual porosity, which follows from the sample microstructure. With an increase in the La_2O_3 content up to 5%, presumably, a perovskite LaYbO_3 phase is formed in ceramics in addition to the cubic one, which causes scattering, especially in the region of short wavelengths.

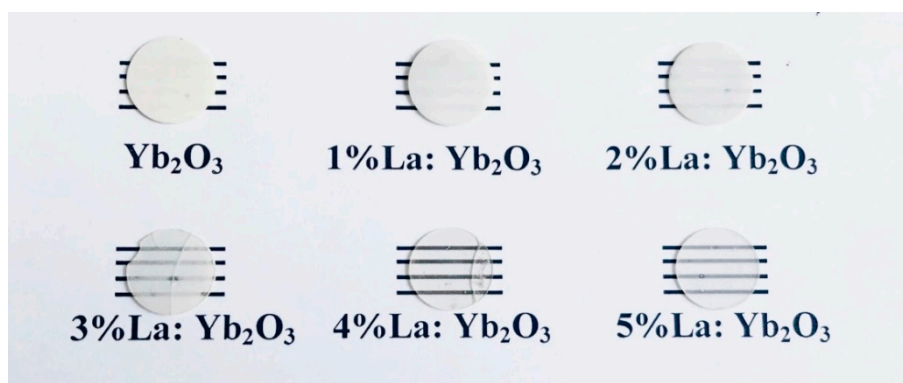


Figure 5. Appearance of La:Yb₂O₃ ceramics sintered in vacuum at 1750 °C.

A sample with the highest transmission (4% La:Yb₂O₃) was chosen to study the optical properties. Figure 6 shows the transmission spectrum of ceramics after vacuum sintering. In-line transmittance for the 4% La sample is maximum in the wavelength range of 5–6 μm and reaches 82.8%. The short-wavelength transmission edge of the La:Yb₂O₃ ceramics is in the region of 270 nm, and the long-wavelength edge is at 8.7 μm . In the near-infrared range there are absorption bands characteristic of the Yb³⁺ ion in the wavelength range of 0.9–1.03 μm .

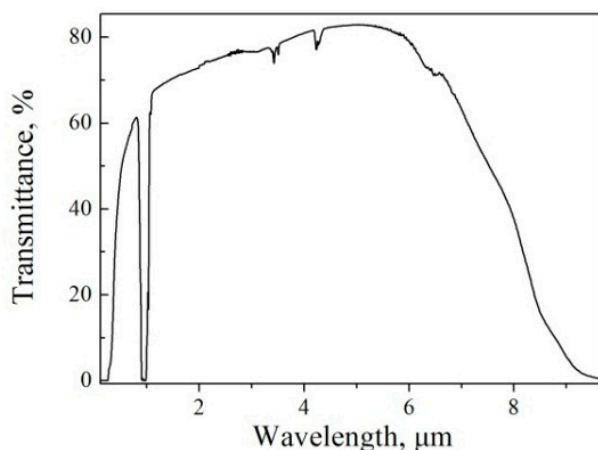


Figure 6. Optical transmission spectrum of 4% La:Yb₂O₃ ceramics.

The results of measuring the Verdet constant for 4% La:Yb₂O₃ ceramics are shown in Figure 7 in comparison with the widely used TGG material (see Figure 7a) and with some other known magneto-optical materials which are transparent in the spectral range beyond 1.4 μm (see Figure 7b). The dependences of the Verdet constant on the wavelength are obtained by approximating experimental data for a TGG single crystal [32], Dy₂O₃ ceramics [20] using the approximation formula from [33], Er₂O₃ ceramics [25], Ho₂O₃ ceramics [24,35], EuF₂, NHF single crystals [36], and for some types of magneto-optical glasses: ternary phosphate glass [37] and TeO₂ [38].

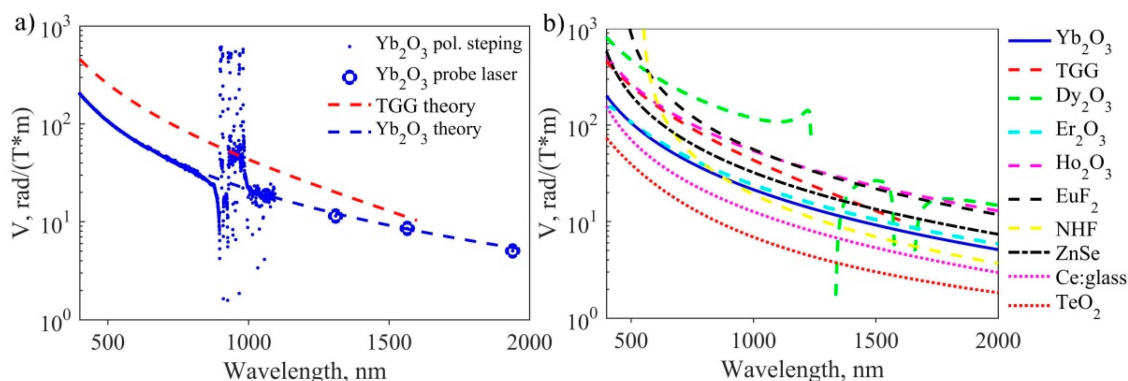


Figure 7. The dependence of the 4%La:Yb₂O₃ Verdet constant on the wavelength (a) in comparison with terbium gallium garnet (TGG) crystal and (b) other previously studied materials.

Dependence of the Verdet constant on the wavelength in the transparency region is well described by the equation $V = A/(\lambda^2 - \lambda_0^2)$, where $A = 2 \times 10^6 \text{ rad}\cdot\text{nm}^2/(\text{T}\cdot\text{m})$, $\lambda_0 = 245 \text{ nm}$ (blue dotted line), and this dependence is very different in the region of absorption bands (0.9–1.1 μm), where it is impossible to use this material as a magneto-optical one.

These approximations do not describe the behavior of the Verdet constant in the regions with absorption and describe well the behavior of the Verdet constant in the wavelength ranges in which the experiment was carried out in each of the works.

Yb₂O₃ ceramics are comparable to the Er₂O₃ material in terms of the Verdet constant and they are better than the presented glasses in the entire transparency range. In the 400–900 nm range, Yb₂O₃ ceramics are inferior to all the remaining listed materials in their magneto-optical properties. A distinctive feature of Yb₂O₃ ceramics from many of the listed materials is the absence of absorption bands in the 1.1–6 μm range and a relatively high value of Verdet constant. All materials containing Tb³⁺ have a long-wavelength absorption edge starting at 1.4 μm; Dy₂O₃ has several absorption lines in the range of 1–1.9 μm and 2.3–3.5 μm; and Er₂O₃ absorption lines are in the range 1.37–1.8, 1.07–1.3, and 1.65–2.2 μm for Ho₂O₃ and 1.06–1.12, 1.21–1.29, and 1.35–1.52 μm for EuF₂. NHF has a transparency window in the range of 1.25–1.69 μm and a lower value of the Verdet constant compared to Yb₂O₃. Thus, use of Yb₂O₃ ceramics as a magneto-optical material is promising in the range of 1.5–1.9 μm due to the fact that the absorption bands are far from this range and the value of the Verdet constant is relatively high. Zinc selenide (ZnSe) has no absorption bands in this range and the value of the Verdet constant is ~1.4 times higher; however, to objectively compare the prospects of these materials for use as Faraday isolators for laser radiation with high average power, it is necessary to compare the mechanical and thermo-optical properties of these materials, which are planned to be studied in the near future.

4. Conclusions

La:Yb₂O₃ powders and optical ceramic samples were obtained for the first time by self-propagating high-temperature synthesis and vacuum sintering. It was shown that addition of 4 mol.% of La₂O₃ enhances the sinterability of Yb₂O₃, improving optical transmission of the ceramics. The prepared ytterbium oxide ceramics are transparent in the 270–900 nm and 1.1–8.7 μm spectral ranges. The resulting 4% La:Yb₂O₃ ceramics have an optical transmission 73% at a wavelength of 2 μm, limited by residual porosity and probably secondary phase enriched with La₂O₃. Due to the distant location of the absorption bands and the relatively high value of the Verdet constant, the use of Yb₂O₃ ceramics as a magneto-optical media in the wavelength range of 1.5–1.9 μm is the most promising at the moment.

Author Contributions: Conceptualization, D.A.P.; methodology, validation, D.A.P., S.S.B., I.L.S., and O.V.P.; formal analysis, D.A.P.; investigation, V.A.K., K.E.S., I.L.S., and A.V.N.; writing—original draft preparation, A.V.N.; writing—review and editing, D.A.P. and S.S.B.; visualization, A.V.N.; supervision, D.A.P. and O.V.P.; project administration, D.A.P. and S.S.B. All authors have read and agreed to the published version of the manuscript.

Funding: The study of magneto-optical properties of Yb₂O₃ was funded by Russian Foundation for Basic Research (RFBR), grant number 18-02-00500 A. The work at IChHPS of RAS was performed within the state assignment No. 0095-2019-0005.

Conflicts of Interest: The authors declare no conflict of interest.

References

- Papp, A.; Harms, H. Magneto-optical current transformer 1: Principles. *Appl. Opt.* **1980**, *19*, 3729–3734. [\[CrossRef\]](#)
- Zhou, F.Z.; Hu, W.T.; Chen, Y.M.; Li, Z.S.; Shen, L.Q.; Fen, X.Q.; Hu, G.Q.; Yin, Z.W. Compact, magneto-optic Q-switched, neodymium-doped bismuth germanate crystal (Nd:BGO) laser pumped by a laser diode. *Appl. Opt.* **1995**, *34*, 4266–4268. [\[CrossRef\]](#)
- Scott, G.; Lacklison, D. Magneto-optic properties and applications of bismuth substituted iron garnets. *IEEE Trans. Magn.* **1976**, *12*, 292–311. [\[CrossRef\]](#)
- Mironov, E.A.; Snetkov, I.; Voitovich, A.V.; Palashov, O.V. Permanent-magnet Faraday isolator with the field intensity of 25 kOe. *Quantum Electron.* **2013**, *43*, 740–743. [\[CrossRef\]](#)
- Mironov, E.A.; Voitovich, A.V.; Palashov, O.V. Permanent-magnet Faraday isolator with the field intensity of more than 3 tesla. *Laser Phys. Lett.* **2019**, *17*, 015001. [\[CrossRef\]](#)
- Khazanov, E.A. Compensation of thermally induced polarisation distortions in faraday isolators. *Quantum Electron.* **1999**, *29*, 59–64. [\[CrossRef\]](#)
- Solomonov, V.I.; Osipov, V.V.; Shitov, V.A.; Maksimov, R.; Lipchak, A.I. Optical properties of ytterbium-doped yttrium oxide ceramics. *Phys. Status Solidi* **2016**, *214*, 1600786. [\[CrossRef\]](#)
- Snetkov, I.; Mukhin, I.; Palashov, O.; Khazanov, E. Compensation of thermally induced depolarization in Faraday isolators for high average power lasers. *Opt. Express* **2011**, *19*, 6366–6376. [\[CrossRef\]](#) [\[PubMed\]](#)
- Snetkov, I.; Voitovich, A.V.; Palashov, O.V.; Khazanov, E.A. Review of Faraday Isolators for Kilowatt Average Power Lasers. *IEEE J. Quantum Electron.* **2014**, *50*, 434–443. [\[CrossRef\]](#)
- Snetkov, I. Features of Thermally Induced Depolarization in Magneto-Active Media with Negative Optical Anisotropy Parameter. *IEEE J. Quantum Electron.* **2018**, *54*, 1–8. [\[CrossRef\]](#)
- Yakovlev, A.; Snetkov, I.L. Thermal Lens Astigmatism Induced by the Photoelastic Effect in m3m, 432, and 43m Symmetry Cubic Crystals. *IEEE J. Quantum Electron.* **2020**, *56*. [\[CrossRef\]](#)
- Balabanov, S.S.; Permin, D.A.; Rostokina, E.Y.; Egorov, S.V.; Sorokin, A.A. Sinterability of nanopowders of terbium solid solutions with scandia, yttria, and lutetia. *J. Adv. Ceram.* **2018**, *7*, 362–369. [\[CrossRef\]](#)
- Ikesue, A.; Aung, Y.L.; Makikawa, S.; Yahagi, A. Total Performance of Magneto-Optical Ceramics with a Bixbyite Structure. *Materials* **2019**, *12*, 421. [\[CrossRef\]](#) [\[PubMed\]](#)
- Aung, Y.L.; Ikesue, A.; Yasuhara, R.; Iwamoto, Y. Magneto-optical Dy₂O₃ ceramics with optical grade. *Opt. Lett.* **2020**, *45*, 4615. [\[CrossRef\]](#) [\[PubMed\]](#)
- Balabanov, S.S.; Demidova, K.; Filofeev, S.; Ivanov, M.; Kuznetsov, D.; Li, J.; Permin, D.A.; Rostokina, E. Influence of Lanthanum Concentration on Microstructure of (Ho_{1-x}La_x)₂O₃ Magneto-Optical Ceramics. *Phys. Status Solidi* **2020**, *257*. [\[CrossRef\]](#)
- Li, X.; Liu, Q.; Liu, X.; Chen, X.; Wu, L.; Xie, T.; Shi, Y.; Chen, H.; Li, J. Novel (Tb_{0.99}Ce_{0.01})₃Ga₅O₁₂ magneto-optical ceramics for Faraday isolators. *Scr. Mater.* **2020**, *177*, 137–140. [\[CrossRef\]](#)
- Veber, P.; Velazquez, M.; Gadret, G.; Rytz, D.; Peltz, M.; Decourt, R. Flux growth at 1230 °C of cubic Tb₂O₃ single crystals and characterization of their optical and magnetic properties. *CrystEngComm* **2015**, *17*, 492–497. [\[CrossRef\]](#)
- Snetkov, I.; Permin, D.A.; Balabanov, S.S.; Palashov, O.V. Wavelength dependence of Verdet constant of Tb³⁺:Y₂O₃ ceramics. *Appl. Phys. Lett.* **2016**, *108*, 161905. [\[CrossRef\]](#)
- Snetkov, I.; Palashov, O. Cryogenic temperature characteristics of Verdet constant of terbium sesquioxide ceramics. *Opt. Mater.* **2016**, *62*, 697–700. [\[CrossRef\]](#)
- Snetkov, I.; Yakovlev, A.I.; Permin, D.A.; Balabanov, S.S.; Palashov, O.V. Magneto-optical Faraday effect in dysprosium oxide (Dy₂O₃) based ceramics obtained by vacuum sintering. *Opt. Lett.* **2018**, *43*, 4041–4044. [\[CrossRef\]](#)
- Yakovlev, A.; Snetkov, I.; Permin, D.; Balabanov, S.; Palashov, O. Faraday rotation in cryogenically cooled dysprosium based (Dy₂O₃) ceramics. *Scr. Mater.* **2019**, *161*, 32–35. [\[CrossRef\]](#)

22. Furuse, H.; Yasuhara, R. Magneto-optical characteristics of holmium oxide (Ho_2O_3) ceramics. *Opt. Mater. Express* **2017**, *7*, 827–833. [\[CrossRef\]](#)
23. Balabanov, S.; Filofeev, S.; Ivanov, M.; Kaigorodov, A.; Kuznetsov, D.; Hu, D.; Li, J.; Palashov, O.; Permin, D.; Rostokina, E.; et al. Fabrication and characterizations of holmium oxide based magneto-optical ceramics. *Opt. Mater.* **2020**, *101*, 109741. [\[CrossRef\]](#)
24. Hu, D.; Li, X.; Snetkov, I.; Yakovlev, A.; Balabanov, S.; Ivanov, M.; Liu, X.; Liu, Z.; Tian, F.; Xie, T.; et al. Fabrication, microstructure and optical characterizations of holmium oxide (Ho_2O_3) transparent ceramics. *J. Eur. Ceram. Soc.* **2020**, *41*, 759–767. [\[CrossRef\]](#)
25. Yakovlev, A.; Balabanov, S.; Permin, D.; Ivanov, M.; Snetkov, I. Faraday rotation in erbium oxide based ceramics. *Opt. Mater.* **2020**, *101*, 109750. [\[CrossRef\]](#)
26. Peters, V. Growth and Spectroscopy of Ytterbium-Doped Sesquioxides. Ph.D. Thesis, University of Hamburg, Hamburg, Germany, 2001.
27. Yagi, H.; Yanagitani, T. Translucent Rare Earth Oxide Sintered Article and Method for Production Thereof. EP 1,336,596 B1, 24 June 2002.
28. Balabanov, S.S.; Bykov, Y.; Egorov, S.; Ereemeev, A.; Gavrishchuk, E.; Khazanov, E.; Mukhin, I.; Palashov, O.; Permin, D.A.; Zelenogorsky, V. Transparent $\text{Yb}:(\text{YLa})_2\text{O}_3$ ceramics produced by self-propagating high-temperature synthesis and microwave sintering. *Opt. Mater.* **2013**, *35*, 727–730. [\[CrossRef\]](#)
29. Snetkov, I.L.; Mukhin, I.B.; Balabanov, S.S.; Permin, D.A.; Palashov, O.V. Efficient lasing in $\text{Yb}:(\text{YLa})_2\text{O}_3$ ceramics. *Quantum Electron.* **2015**, *45*, 95–97. [\[CrossRef\]](#)
30. Permin, D.A.; Balabanov, S.; Novikova, A.; Snetkov, I.; Palashov, O.; Sorokin, A.; Ivanov, M. Fabrication of Yb-doped Lu_2O_3 - Y_2O_3 - La_2O_3 solid solutions transparent ceramics by self-propagating high-temperature synthesis and vacuum sintering. *Ceram. Int.* **2019**, *45*, 522–529. [\[CrossRef\]](#)
31. Permin, D.; Balabanov, S.; Snetkov, I.; Palashov, O.; Novikova, A.; Klyusik, O.; Ladenkov, I. Hot pressing of $\text{Yb}:\text{Sc}_2\text{O}_3$ laser ceramics with LiF sintering aid. *Opt. Mater.* **2020**, *100*, 109701. [\[CrossRef\]](#)
32. Snetkov, I.; Yasuhara, R.; Starobor, A.V.; Mironov, E.A.; Palashov, O.V.; Starobor, A. Thermo-Optical and Magneto-Optical Characteristics of Terbium Scandium Aluminum Garnet Crystals. *IEEE J. Quantum Electron.* **2015**, *51*, 1–7. [\[CrossRef\]](#)
33. Slezák, O.; Yasuhara, R.; Vojna, D.; Furuse, H.; Lucianetti, A.; Mocek, T. Temperature-wavelength dependence of Verdet constant of Dy_2O_3 ceramics. *Opt. Mater. Express* **2019**, *9*, 2971–2981. [\[CrossRef\]](#)
34. Flores, J.L.; Ferrari, J.A. Verdet constant dispersion measurement using polarization-stepping techniques. *Appl. Opt.* **2008**, *47*, 4396–4399. [\[CrossRef\]](#) [\[PubMed\]](#)
35. Vojna, D.; Yasuhara, R.; Furuse, H.; Slezák, O.; Hutchinson, S.; Lucianetti, A.; Mocek, T.; Cech, M. Faraday effect measurements of holmium oxide (Ho_2O_3) ceramics-based magneto-optical materials. *High Power Laser Sci. Eng.* **2018**, *6*, 6. [\[CrossRef\]](#)
36. Starobor, A.; Mironov, E.; Volkov, M.; Karimov, D.; Ivanov, I.; Lovchev, A.; Naumov, A.; Semashko, V.; Palashov, O. Thermal lens investigation in EuF_2 , PrF_3 , and $\text{Na}_{0.38}\text{Ho}_{0.62}\text{F}_{2.24}$ crystals for magneto-optical applications. *Opt. Mater.* **2020**, *99*, 109542. [\[CrossRef\]](#)
37. Babkina, A.; Kulpina, E.; Sgibnev, Y.; Fedorov, Y.; Starobor, A.; Palashov, O.; Nikonorov, N.; Ignatiev, A.; Zyryanova, K.; Oreshkina, K.; et al. Terbium concentration effect on magneto-optical properties of ternary phosphate glass. *Opt. Mater.* **2020**, *100*, 109692. [\[CrossRef\]](#)
38. Yakovlev, A.; Snetkov, I.; Dorofeev, V.; Motorin, S.E. Magneto-optical properties of high-purity zinc-tellurite glasses. *J. Non-Cryst. Solids* **2018**, *480*, 90–94. [\[CrossRef\]](#)

Publisher’s Note: MDPI stays neutral with regard to jurisdictional claims in published maps and institutional affiliations.



© 2020 by the authors. Licensee MDPI, Basel, Switzerland. This article is an open access article distributed under the terms and conditions of the Creative Commons Attribution (CC BY) license (<http://creativecommons.org/licenses/by/4.0/>).